Research Article

BRJ
Biomedical Research Journal

Biomagnetic Interaction of Functionalized Iron Oxide Nanoparticles with Bovine Serum Albumin

Mayank Gupta[1] and Sudeshna Chandra[2]*

[1]Department of Metallurgical Engineering and Materials Science, Indian Institute of Technology Bombay, Powai, Mumbai – 400076, India.
[2]Department of Chemistry, Sunandan Divatia School of Science, SVKM's NMIMS University, Vile Parle (West) Mumbai – 400056, India.

Functionalized iron oxide (magnetic) nanoparticles are promising candidate for detection and sensing of target molecule as they can be manipulated and detected through magnetic interactions. The biological recognition moiety of the functionalized coating results in binding of the target analyte which causes a change in the interaction of the nanoparticles under the influence of an external magnetic field. This forms the basis of the fabrication of a bio-magnetic sensor. The current study reports the use of three different macromolecules viz. glycol chitosan (GC), poly ethylene glycol methyl ether (PEGME) and poly sodium stereo-4 sulphate (PSSNa) to functionalize and cap the magnetic nanoparticles. The magnetic nanoparticles were characterized using FTIR, XRD, TEM and TGA to evaluate their structural and surface properties. TEM showed spherical nanoparticles with mean size of ~11, 12 and 13 nm for GC, PEGME and PSSNa-MNPs respectively. TGA evaluates the weight loss of the modified MNPs and confirms the coating on the surface of the MNPs. Bovine serum albumin (BSA) was immobilized on the functionalized MNPs and detection studies were carried out using AC susceptibility studies on a physical property measurement system. Detection of BSA immobilized MNPs was exhibited at 300 K by the measurement of the imaginary part of the magnetic susceptibility over a frequency range and is based on the changes of dynamic magnetic properties of the MNPs, making use of the Brownian relaxation.

INTRODUCTION

Magnetic nanoparticles (MNPs) are of interest to researchers for applications in magnetic fluids (Chikazumi *et al.,* 1987), catalysis (Lu *et al.,* 2004; Tsang *et al.,* 2004), biotechnology/biomedicine (Gupta and Gupta, 2005), magnetic resonance imaging (Mornet *et al.,* 2006; Li *et al.,* 2005), data storage (Hyeon, 2003), and environmental remediation (Elliott and Zhang, 2001). MNPs can also be manipulated under the influence of an external magnetic field. Of the several MNPs, iron oxides are unique due to their non-toxicity, biocompatibility and injectability, indicating biomedical applications like magnetic resonance

Key words: Magnetic nanoparticles, bio-magnetic sensors, AC susceptibility, macromolecules, Brownian relaxation.
***Corresponding Author:** Sudeshna Chandra, Department of Chemistry, Sunandan Divatia School of Science, SVKM's NMIMS University, Vile Parle (West) Mumbai, 400056, India.
Email: sudeshna.chandra@nmims.edu

imaging (MRI), targeted drug and gene delivery, tissue engineering, cell tracking and magnetic bioseparation (Shubayev *et al.,* 2009). Iron oxide nanoparticles after being loaded with drugs and bioactive agents such as peptides and nucleic acids, form distinct particulate systems that may penetrate cell and tissue barriers. This property enables applications in organ-specific therapeutics and diagnostic modalities (McCarthy *et al.,* 2007).

An unavoidable problem associated with nanosized iron oxide nanoparticles is the intrinsic instability for longer duration, due to the tendency to form aggregates thereby reducing surface energy. Further, the bare metallic nanoparticles are easily oxidized in air resulting in loss of magnetism and dispersibility. Hence, it is important to chemically stabilize the bare magnetic nanoparticles against degradation and agglomeration during or after synthesis, for use in various applications. This can be achieved by grafting/coating the nanoparticles with organic species, like surfactants or polymers, or inorganic materials, such as silica or carbon. The protecting materials serves dual purpose by stabilizing the nanoparticles and by providing functionalities for attachment of various ligands.

The MNPs' ability to be functionalized and the property to respond to an external magnetic field provides a useful tool for sensing and detection of target biomolecules. The biological recognition function of the functionalized MNPs results in binding of the target analyte which causes a change in the interaction of the particle in presence of an external magnetic field. These sensors detect changes in the stray magnetic field of functionalized MNPs upon binding with the target analyte. The magnetic field sensors are based on anisotropic magnetoresistance (Miller *et al.,* 2002), Hall Effect (Besse *et al.,* 2002), or spin valves (Ferreira et al., 2003; Kemp *et al.,* 2003). Alternatively, a superconducting quantum interference device (SQUID) may be used to detect the biological binding activity through relatively slow magnetic Néel relaxation upon immobilization of the biomagnetic particles (Haller *et al.,* 1999). However, this type of sensing does not discriminate different targets of similar biological binding affinity. A new sensing scheme recently devised, makes use of the Brownian relaxation of magnetization of MNPs (Chung *et al.,* 2003). The dominant relaxation mechanism of magnetization of the particle depends on size of the particle.

For particles less than 10 nm, Néel relaxation is the dominant mechanism, whereas for larger particles, Brownian relaxation is dominant.

Study of the AC susceptibility of nanoparticles is performed by plotting the imaginary part of the complex magnetic susceptibility against the frequency. The frequency at which the peak in the imaginary part of the complex magnetic susceptibility is obtained, is characteristic of size of the nanoparticles. By measuring the change in frequency on addition of the target analyte, change in size of the particle is measured and hence the target analyte is detected. Use of an ideal functional agent which binds to a particular target analyte of known size, helps in its detection by overcoming the inherent weakness present in other magnetic field sensors.

The motivation for the study is to utilize the selective bio-affinity of the functional moiety and magnetic properties of MNPs to design a sensor to detect target bio-molecules. The sensor is based on changes of dynamic magnetic properties of the MNPs using the Brownian relaxation.

EXPERIMENTAL

Materials used

Ferric chloride hexahydrate ($FeCl_3.6H_2O$), ferrous chloride tetrahydrate ($FeCl_2.4H_2O$), sodium hydroxide, glycol chitosan, poly ethylene glycol methyl ether, poly sodium stereo-4-sulfate and bovine serum albumin (BSA) were procured from Sigma Aldrich, India. 100% ethanol solution used for washing precipitates was obtained from Baker Hughes, India. All other chemicals were of analytical grade and were procured from Loba Chemie Pvt. Ltd., India and used as received. Deionized water was used as the solvent.

The capping agents used were glycol chitosan (GC), poly ethylene glycol methyl ether (PEGME) and poly sodium stereo-4-sulfate (PSSNa).

Preparation of Functionalized Iron Oxide Nanoparticles

The magnetic nanoparticles were prepared by the conventional co-precipitation method with a 2:1 molar ratio of Fe^{3+}/Fe^{2+}. 3 g of $FeCl_3.6H_2O$ and 1.05 g of $FeCl_2.4H_2O$ was dissolved in 40 ml of deionised water and was stirred in a five-necked flask under nitrogen atmosphere for 30–45 min at 500–600 rpm until a temperature of 80°C was reached. 5 M NaOH (10 ml) was added dropwise till the solution turned from orange to black. The reaction mixture was then stirred

vigorously at 800–1000 rpm for 1 h. This was repeated three times, once for each capping (functional) agent. To each reaction mixture, 20 ml of capping agent solution (50 mg/ml concentration) was added 30 minutes prior to completion, following which the system was allowed to cool to room temperature. The solutions obtained were washed alternatively with deionised water and ethanol, and supernatants removed by decantation using a permanent magnet to separate the magnetic precipitates. The resultant black powders were dried at 40–50°C in a vacuum oven. The overall reaction was as follows: $Fe^{2+} + 2Fe^{3+} + 8OH^{-} \rightarrow Fe_3O_4 + H_2O$

The obtained MNPs as stabilized by the capping agents are henceforth referred GC-MNPs, PEGME-MNPs and PSSNa-MNPs.

Immobilization of BSA on functionalized MNPs

50 mg of functionalized MNPs and 50 mg BSA were dispersed in 100 mL deionised water and stirred for 5 hours. The suspension was washed with deionised water, three times. The solution was then centrifuged at 10000 rpm for 10–15 min and the supernatant removed by decantation. The resultant black powder was dried at 40–50°C in a vacuum oven. The resultant nanoparticles are named as BSA-GC-MNPs, BSA-PEGME-MNPs, BSA-PSSNa-MNPs.

Characterization Techniques

The phase purity and identification of the MNPs were done by X-ray diffraction (XRD) with PanAnalytical X-Pert diffractometer using a monochromatised X-ray beam with nickel-filtered Cu-Kα radiation at 4°/min scan rate. Fourier transform infrared (FT-IR) spectra were obtained using Jasco, FT-IR 300E spectrometer with a resolution of 4 cm^{-1}. The TEM micrographs were observed by JEOL JEM 2100 for particle size determination. The thermal analysis of the system was carried out by Thermogravimetric analysis (SDT Q 600). Magnetic properties of MNPs were studied using Vibrating Sample Magnetometer Model: 7410, Lake Shore Cryotonics Inc., Ohio, U.S.A.

Magnetic studies of BSA immobilized functional MNPs

Physical Property Measurement System (PPMS) and Magnetic Property Measurement System (MPMS) from Quantum Design was used to study the magnetic behavior of the BSA immobilized MNPs. PPMS was

configured to detect the magnetic moment of the sample material, from which various magnetic parameters like magnetization, magnetic susceptibility were determined. For the MPMS, superconductivity is the critical enabling technology that provides for production of large, stable magnetic fields, and the ability to measure changes in those fields 14 orders of magnitude smaller. Known weight of powder samples were coated in Teflon and were given for testing.

RESULTS AND DISCUSSION

The samples GC-MNPs, PEGME-MNPs and PSSNa-MNPs were synthesized using a co-precipitation reaction. The functionalized MNPs were characterized by FTIR, XRD, TEM and TGA to evaluate their structural and surface properties. Bovine serum albumin (BSA) as exemplary protein was immobilized on the functionalized MNPs to evaluate performance of the MNPs for use as platform for biomagnetic sensing.

The FTIR spectra of GC and GC-MNPs is given in Fig. 1a. The absorption bands for GC were well resolved, whereas those of GC-MNPs were rather broad and few. The CC stretching peaks of the alkyl chains of GC at 1604 cm^{-1} and 1380 cm^{-1} shifted to 1618 cm^{-1} and 1367 cm^{-1},

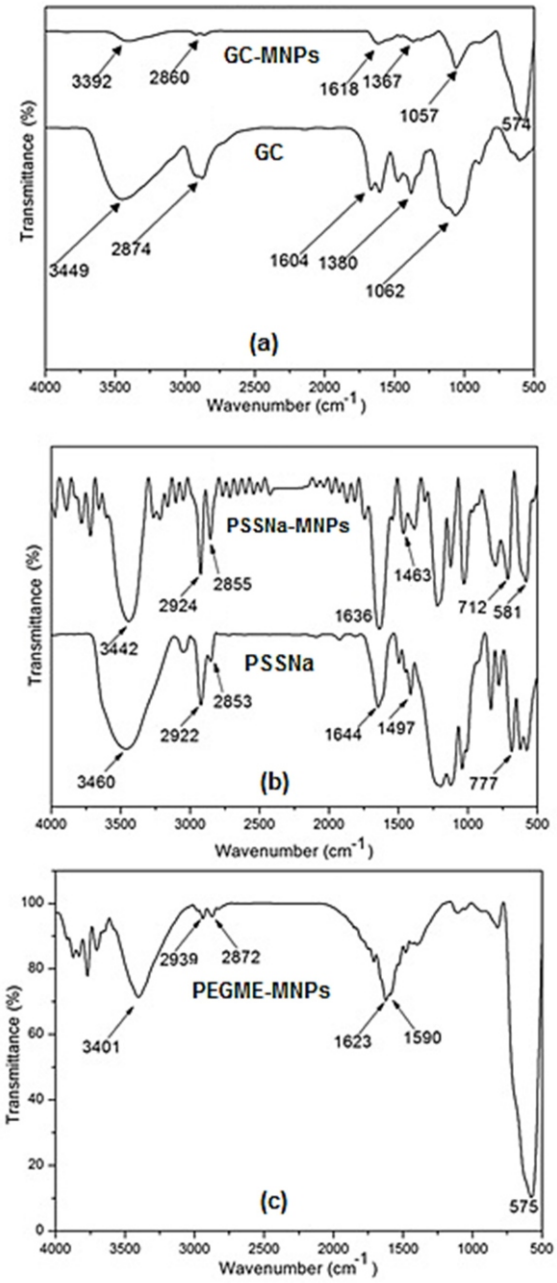

Figure 1. FTIR spectra of (a) GC and GC-MNPs (b) PSSNa and PSSNa-MNPs and (c) PEGME- MNPs.

respectively in GC-MNPs. The peaks at 1062 cm^{-1} and 1057 cm^{-1} are assigned to the CO stretching of the ether bonds. The OH and NH stretching vibrations were observed at 3449 cm^{-1} and 3392 cm^{-1} respectively, while the sharp peaks at 2874

cm^{-1} and 2860 cm^{-1} corresponded to asymmetric and symmetric CH_2 stretching modes. The peak at 3449 cm^{-1} due to NH stretching vibrations appeared broader with a shift at 3392 cm^{-1} in GC-MNPs, indicating that binding of GC to Fe_3O_4 nanoparticles takes place through the amine functionality. Possibly, amine groups of GC form complexes with the Fe-atoms on surface of Fe_3O_4 nanoparticles, weakening the amine bond thereby shifting to lower frequencies.

The FTIR spectra of PSSNa and PSSNa-MNPs is shown in Fig. 1b. The peaks at 1497 cm^{-1} and 1413 cm^{-1} can be assigned to S=O (asymmetric stretching) of the sulfonate bonds. These peaks shift to broad bands at 1463 cm^{-1} and 1387 cm^{-1} in PSSNa-MNPs revealing binding of PSSNa to Fe_3O_4 nanoparticles through sulfonate functionality. The peaks at 2922, 2853, 2924, and 2855 cm^{-1} corresponded to the asymmetric and symmetric CH_2 stretching modes. The peaks at 1644 cm^{-1} and 1636 cm^{-1} are assignable to the CC stretching of benzene ring. The peak at 777 cm^{-1} corresponding to SO stretching of the sulfonate bond in PSSNa shifted to 712 cm^{-1} in PSSNa-MNPs indicating an increase in strength of the bond and suggest bonding of the capping agent to the Fe_3O_4 nanoparticles by sulfonate functionality.

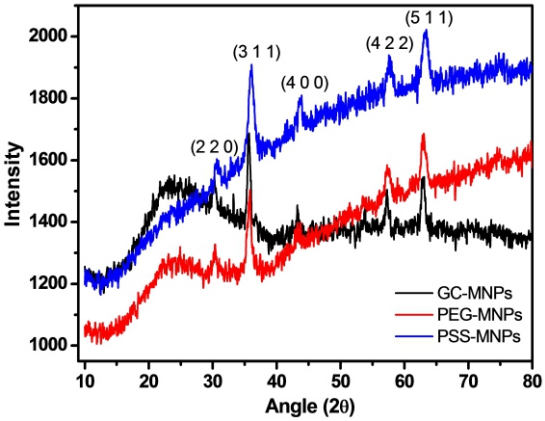

Figure 2. XRD pattern of the functionalized MNPs.

The FTIR spectra of PEGME functionalized MNPs is shown in Fig. 1c. The FTIR analysis of pure PEGME was not possible since PEGME is a waxy material and it could not be powdered along with KBr, for analysis. The peaks obtained at 2939 and 2872 cm^{-1} correspond to the asymmetric and symmetric CH_2 stretching modes (Rufino *et al.,* 2003). The peaks at 1623 cm^{-1} and 1590 cm^{-1} are assigned to the CC stretching of the alkyl chains. The functionalized MNPs showed strong absorption band at ~575 cm^{-1} ascribed to Fe-O stretching vibrational mode of Fe_3O_4 (Ahn *et al.,* 2003).

The XRD pattern of the GC-MNPs, PEGME-MNPs and PSSNa-MNPs (Fig. 2) shows diffraction peaks for planes corresponding to (220), (311), (400), (422), (511) and (440) at 30.4°, 35.5°, 43.2°, 53.8°, 57.3°, 62.7°; 30.4°, 36°, 43.6°, 53.4°, 57.5°, 63.3° and 30.4°, 35.8°, 43.7°, 53.6°, 57.5°, 62.9° 2θ respectively. The data indicates formation of single-phase Fe_3O_4

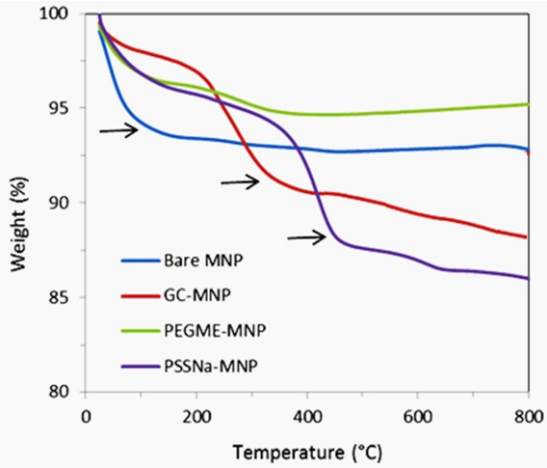

Figure 3. TGA Curves of bare and functionalized MNPs.

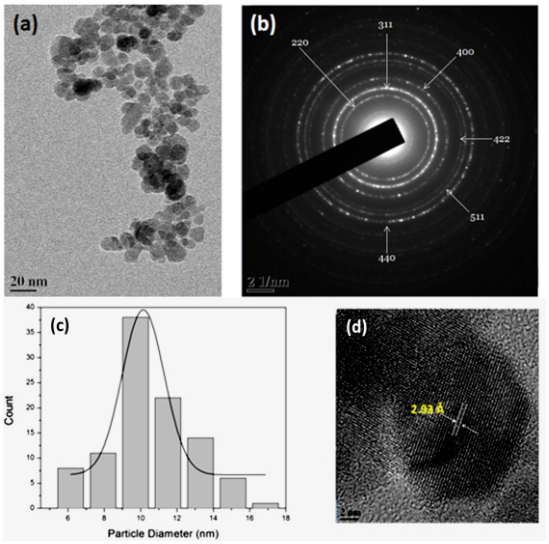

Figure 4. (a)TEM and (b) Electron diffraction pattern (c) particle histogram and (d) HRTEM of GC- MNPs.

inverse spinel structure in the three functionalized MNPs with lattice constants a = 8.37 Å, a = 8.27 Å and a = 8.30 Å respectively, close to reported value of magnetite (JCPDS card No. 88-0315, a = 8.375 Å). The presence of sharp and intense peaks confirms formation of highly crystalline nanoparticles.

The thermogravimetric analysis (TGA) of bare Fe_3O_4, GC-MNPs, PEGME-MNPs and the PSSNa-MNPs are shown in Fig. 3, indicating one weight loss process in Fe_3O_4. The weight loss (~6%) at 100°C is ascribed to the evaporation of adsorbed water molecules.

The functionalized MNPs indicated two weight loss processes, including removal of water below 100°C and an additional weight loss which occurs from 200–400°C assigned to removal of the organic capping agent, as the capping agents burn out at temperatures near 250ºC. At ~550°C, the weight of the sample remained constant and weight loss after this temperature was not observed. It has been observed that the weight loss of bare MNPs are more than the PEGME-MNPs which may be due to delayed combustion brought about by increase in the oxidation temperature. This is caused by their interaction with metal oxide nanoparticles [Karaŏglu *et al*., 2011]. PEG combustion starts at ~340°C and is completely combusted at ~400°C. Further, PEG is not associated with water molecules, hence the weight loss due to water is not observed in contrast to the bare MNPs.

The TEM image of GC-MNPs shows that the particles are spherical although irregular in shape (Fig. 4a). Electron diffraction (Fig. 4b) revealed dense ring

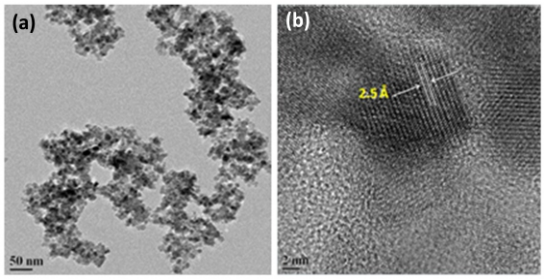

Figure 5. (a) TEM image and (b) HRTEM of PEGME-MNPs.

patterns with d-spacings of 2.94, 2.51, 2.10, 1.70, 1.60, 1.47 Å, matching standard body centered cubic spinel structure (JCPDS card No. 88-0315). The histogram of size distribution of the GC-MNPs (Fig. 4c) showed the mean size of MNPs as 11.41 ± 0.13 nm. The results were similar as with XRD results. Fig. 4d shows the HRTEM image of GC-MNPs. The crystallite in the image has d-spacing of 2.94 Å corresponding to the (220) plane of Fe_3O_4.

The TEM image of PEGME-MNPs also showed the particles as spherical although irregular in shape (Fig. 5a). The mean size of the MNPs is 12.91 nm ± 0.13 nm. Fig. 5b shows the HRTEM image PEGME-MNPs. The crystallite in the image has d-spacing of 2.5 Å corresponding to the (331) plane of Fe_3O_4. In PSSNa-MNPs, HRTEM image shows the crystallite d-spacing is 2.93 Å corresponding to the (220) plane of Fe_3O_4.

Detection studies of BSA immobilized MNPs

To study the immobilization of BSA on the functionalized MNPs, a magnetic sensor scheme based on the changes of dynamic magnetic properties of magnetic nanoparticles suspended in liquids was used. The sensor scheme employed is based on the detection of dynamic magnetic properties (Pankhurst *et al.,* 2003). The nanoparticles were subjected to a small alternating magnetic field with varying frequency. The imaginary part of the magnetic response exhibited by nanoparticles to AC magnetic field with frequency (ω) was recorded. The magnetic response exhibited was expressed by a complex magnetic susceptibility χ.

The imaginary part of the complex magnetic susceptibility (χ′′) corresponds to the out-of-phase response and is expressed as

$$\chi''(\omega) = \frac{\chi_0 \omega\tau}{1 + (\omega\tau)^2}$$

Where χ_0 is the DC magnetic susceptibility and τ is the effective magnetic relaxation time of MNPs.

The value of this imaginary part (χ″) peaks when $\omega = \tau^{-1}$. The effective magnetic relaxation time is proportional to the volume of the MNPs.

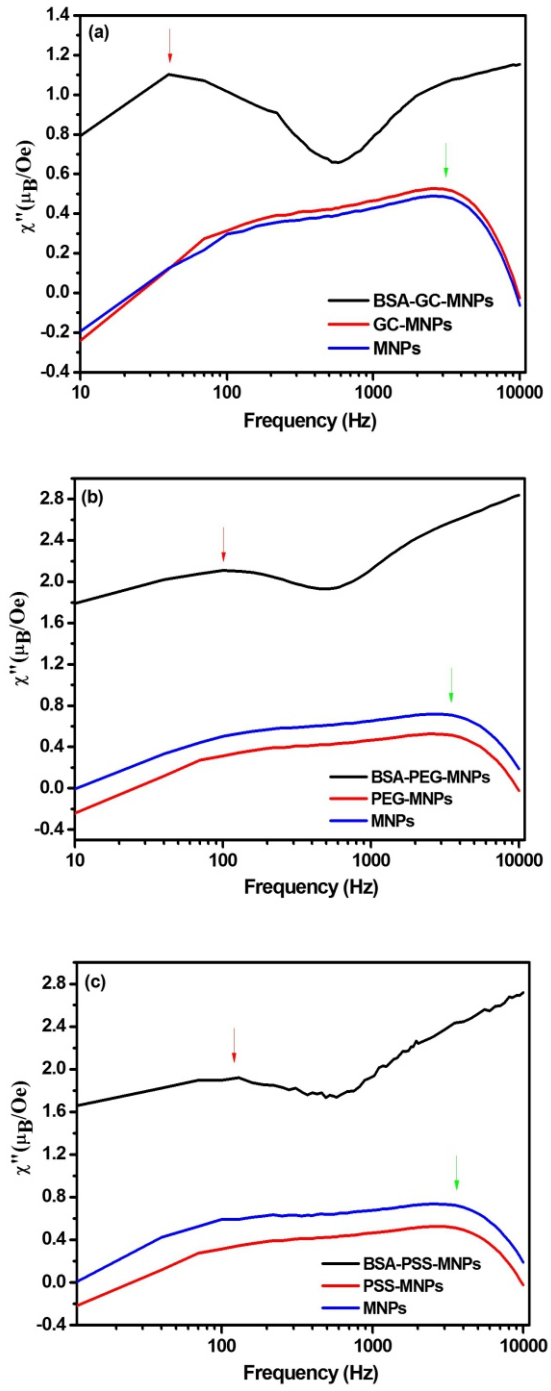

Figure 6. AC susceptibility curves of (a) GC functionalized MNPs (b) PEG functionalized MNPs and (c) PSSNa functionalized MNPs at 300 K at an amplitude of 10 Oe.

PPMS was used to detect immobilization of BSA on the functionalized MNPs by using the above equations. The imaginary part of AC magnetic susceptibility is plotted against frequency. The frequency is varied from 10 Hz to 10,000 Hz while keeping amplitude constant at 10 Oe. These measurements are carried out at two different temperatures viz., 300 K and 10 K. The plot of the imaginary part of the magnetic susceptibility of bare MNPs varies from 0 to 0.25 over the frequency range. The peak value of 0.5 at a frequency of 1250 Hz is shown in Fig. 6. The functionalized MNPs show a very similar parallel plot with a slight offset in values. The offset is a result of a change in the DC magnetic susceptibility of the nanoparticles due to addition of functional agents (Marcon *et al.,* 2012).

At 300 K, decrease in frequency for the peak value of the imaginary part of AC magnetic susceptibility was observed (Fig. 7a-c). The decrease in frequency corresponds to increase in diameter of the functionalized MNPs upon BSA immobilization (Table 1). The increase in diameter corresponds to the size of the BSA molecule, estimated to be 14 nm. An increase in absolute values of AC magnetic susceptibility was observed on addition of BSA. The increase is a result of increase in the DC magnetic susceptibility of the nanoparticles due to immobilization of

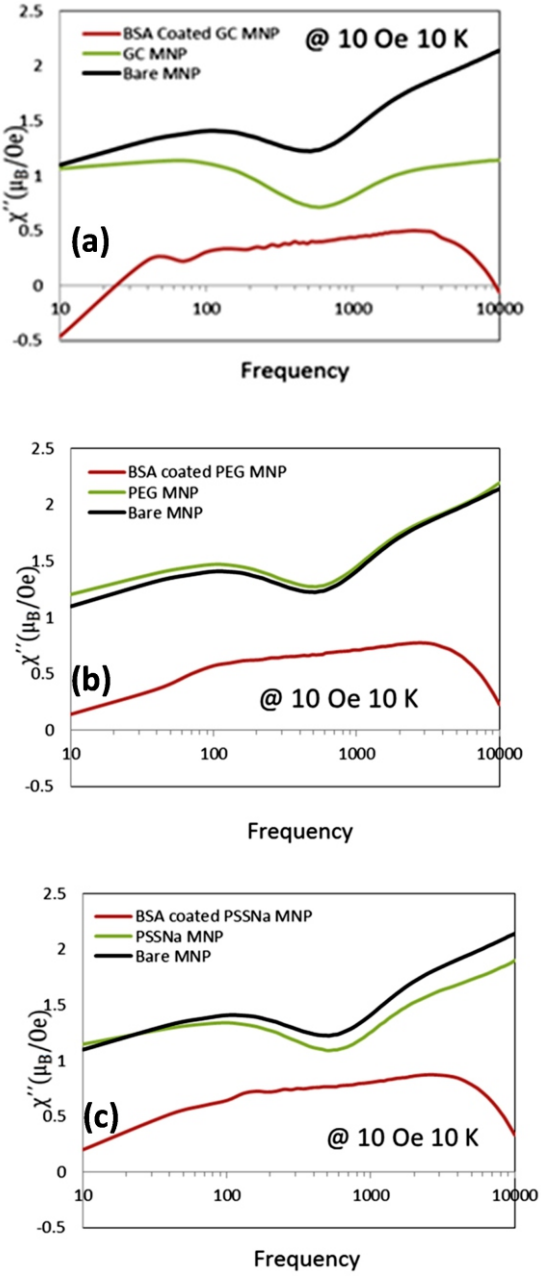

Figure 7. AC susceptibility curves of (a) GC functionalized MNPs (b) PEG functionalized MNPs and (c) PSSNa functionalized MNPs at 10 K and amplitude of 10 Oe.

BSA. DC magnetic susceptibility of a composite particle is a sum of individual DC magnetic susceptibilities of the components.

At 10K, the peak disappeared as shown in Figure 7, due to the fact that 10K is below the freezing point of the liquid. This causes the nanoparticles to be trapped in position in the frozen solution resulting in disappearance of the peak. This also implies that the low frequency peak at room temperature (300K) is due to the rotational diffusive Brownian relaxation of the magnetization.

Table 1. Increase in diameter of functionalized MNPs after immobilization of BSA at 300K and amplitude of 10 Oe.

Functionalized MNPs	Initial Diameter of MNPs (TEM)	Diameter after immobilizing BSA (from AC susceptibility results)	Increase in size
GC – MNPs	11.41 nm	45.28 nm	33.87 nm
PEGME – MNPs	12.91 nm	42.51 nm	29.60 nm
PSSNa – MNPs	13.62 nm	42.02 nm	28.40 nm

CONCLUSIONS

In the current study, magnetic nanoparticles (MNPs) were synthesized and functionalized with macromolecules. The average size of the nanoparticles was below 15 nm. BSA was immobilized on the functionalized MNPs and detection studies were carried out using AC susceptibility studies on a physical property measurement system. Detection of BSA immobilization by functionalized MNPs was exhibited at 300K by the measurement of the imaginary part of the magnetic susceptibility over a frequency range.

ACKNOWLEDGEMENTS

Authors acknowledge the Department of Science and Technology (DST), Govt. of India for providing financial support (Ref. No. SR-WOS-A/CS-45/2010).

CONFLICT OF INTEREST

The authors claim no conflict of interest.

REFERENCES

Ahn Y, Choi EJ, Kim EH, Superparamagnetic relaxation in cobalt ferrite nanoparticles synthesized from hydroxide carbonate precursors. *Rev Adv Mater Sci* 2003;5:477–480.

Besse PA, Boero G, Demierre M, Pott V, Popovic R, Detection of a single magnetic microbead using a miniaturized silicon Hall sensor. *Appl Phys Lett* 2002; 80:4199–4201.

Chikazumi S, Taketomi S, Ukita M, Mizukami M, Miyajima H, Setogawa M, Kurihara Y, Physics of magnetic fluids. *J Magn Mater* 1987;65:245–248.

Chung SH, Hoffmann A, Bader SD, Biological sensors based on Brownian relaxation of magnetic nanoparticles. *Appl Phys Lett* 2003;85:2971–2973.

Elliott DW, Zhang WX, Field assessment of nanoscale bimetallic particles for groundwater treatment. *Environ Sci Technol* 2001; 35:4922–4926.

Ferreira HA, Graham DL, Freitas PP, Cabral JMS, Biodetection using magnetically labeled biomolecules and arrays of spin valve sensors. *J Appl Phys* 2003;93:7281–7286.

Gupta AK, Gupta M, Synthesis and surface engineering of iron oxide nanoparticles for biomedical applications. *Biomaterials* 2005;26:3995–4021.

Haller A, Hartwig S, Matz H, Lange J, Rheinländer T, Kötitz R, Weitschies W, Trahms L, Magnetic relaxation measurement in immunoassay using high-transition-temperature superconducting quantum interference device system. *Supercond Sci Technol* 1999;12:953–955.

Hyeon T, Chemical synthesis of magnetic nanoparticles. *Chem Commun* 2003;32:927–934.

Karaðglu E, Deligöz H, Sözeri H, Baykal A, Toprak MS, *Nano-Micro Lett* 2011;3:25–33.

Kemp JT, Webb C, Davis RW, Sun S, Detection of single micron-sized magnetic bead and magnetic nanoparticles using spin valve sensors for biological applications. *J Appl Phys* 2003;93:7557–7559.

Li Z, Wei L, Gao MY, Lei H, One-Pot Reaction to Synthesize Biocompatible Magnetite Nanoparticles. *Adv Mater* 2005;17:1001–1005.

Lu AH, Schmidt W, Matoussevitch N, Pnnermann HB, Spliethoff B, Tesche B, Bill E, Kiefer W, Schuth F, Nanoengineering of a magnetically separable hydrogenation catalyst. *Angew Chem* 2004;116:4403–4406.

Marcon P, Ostanina K, Overview of Methods for Magnetic Susceptibility Measurement. *PIERS Proceedings* 2012;420–424.

McCarthy JR, Kelly KA, Sun EY, Weissleder R, Targeted delivery of multifunctional magnetic nanoparticles. *Nanomed* 2007;2:153–167.

Miller MM, Prinz GA, Cheng SF, Bounnak S, A model for a magnetoresistance-based biosensor. *Appl Phys Lett* 2002;81:2211–2213.

Mornet S, Vasseur F, Grasset P, Verveka G, Goglio A, Demourgues J, Portier E, Duguet EP, Magnetic nanoparticles design for medical application. *Prog Solid State Chem* 2006;34:237–247.

Pankhurst QA, Connolly J, Jones SK, Dobson J, Applications of magnetic nanoparticles in biomedicine. *J Phys D* 2003;36:167–181.

Rufino ES, Monteiro EEC, Infrared study on methyl metha-crylate-methacrylic acid copolymers and their sodium salts. *Polymer* 2003;44:7189–7198.

Shubayev VI, Pisanic TR, Jin S, Magnetic nanoparticles for theragnostics. *Adv Drug Deliv Rev* 2009;61:467–477.

Takafuji M, Ide S, Ihara H, Xu Z, Preparation of Poly(1-vinylimidazole)-Grafted Magnetic nanoparticles and their application for removal of metal ions. *Chem Mater* 2004;16:1977–1983.

Tsang SC, Caps V, Paraskevas I, Chadwick D, Thompsett D, Magnetically Separable, Carbon-Supported Nanocatalysts for the Manufacture of Fine Chemicals. *Angew Chem Int Ed* 2004;43:5645–5649.